Simulation of High-Frequency Integrated Circuits Incorporating Full-Wave Analysis of Microstrip Discontinuities

Robert Kipp, Chi H. Chan, Andrew T. Yang, and Jack T. Yao

Abstract— **We incorporate full-wave simulation of microstrip interconnects into circuit analysis and show how predicted responses diverge from those based on models from a modern microwave-circuit CAD package. A method is presented for characterizing microstrip interconnects and discontinuities through the method-of-moments applied to a mixed-potential integral equation. The speed is greatly improved though the use of a recently published techniques for rapid evaluation of microstrip spatial Green's functions. A microstrip circuit element is analyzed separately through this procedure, and scattering parameters are extracted from the computed current density. These parameters are passed to a circuit simulator, where small- and large-signal analysis reveal how differences in interconnect modeling affect predicted responses.**

I. Introduction

The increasing speeds and frequencies of analog and digital integrated circuits has generated greater interest in the use of microstrip structures in the interconnects among discrete elements. The development of appropriate design guidelines requires analysis techniques which incorporate into circuit simulation the frequency-dependent effects of these structures. While existing microwave-circuit CAD packages can include microstrip sections in their analyses, these are handled through lumped capacitance and inductance models, quasi-static models, or empirically based closed-form expressions which often fail to account for radiation and other high-frequency phenomena of microstrip. A more rigorous approach is to analyze the structure without simplifying low-frequency or quasi-static approximations, often referred as full-wave analysis.

Much research has been directed toward the full-wave modeling of microstrip interconnects and discontinuities [1]–[3]. One approach is finite-differences time-domain (FDTD) whereby the substrate between the upper conductor and the ground plane is subdivided into a mesh and electromagnetic waves are propagated in time and space through the substrate subject to boundary conditions [4]. Another is method-of-moments (MOM) applied to a relevant integral equation [1], [5], [6].

We confine our analysis to the MOM approach, the details of which are discussed in section II. In this application, MOM involves constructing and solving an impedance matrix whose elements are the mutual impedances among subdivided sections of the microstrip surface conductor. Owing to the nature of the basic microstrip geometry, generating these impedances in a full-wave analysis is often more time consuming than solving the resulting matrix. However, by employing a technique developed in [7], [8] and briefly described in this paper, this process of filling the impedance matrix is accelerated to the point where matrix inversion dominates the solution process.

The MOM procedure yields current distributions for a given set of port excitations. We briefly describe in section III a method for extracting the scattering parameters and transmission-line characteristic impedance from the current. With these data, the microstrip structure is made accessible to circuit simulation. Analysis of a microstrip stub structure is compared with experimental results to validate the overall approach.

In Section IV, small- and large-signal circuit analyses are applied to a microwave amplifier. A harmonic-balance technique used for large-signal simulation is briefly described. The amplifier includes a microstrip meander, a MESFET transistor, and several lumped elements. The meander, which serves as a filtering element, is analyzed both by Libra version 3.000, a commercial microwave CAD package, and the full-wave model outlined below. Circuit simulation is performed by MISIM (Model-Independent Simulator), which employs the computed meander S-parameters and parametric data from the other elements. In the simulation, divergence in predicted performance based on the full-wave modeling and results from Libra is evident at higher frequencies.

II. Modeling Microstrip Discontinuities

A. Computing the Current Distribution

Fig. 1 shows the basic microstrip geometry with an arbitrary strip structure on the surface. The space above the dielectric is unbounded. Simplifying assumptions include an isotropic and horizontally-unbounded dielectric layer, a ground plane with zero resistivity, and an infinitely thin upper conductor with zero resistivity. The method may be extended to incorporate multiple dielectric and strip layers, ohmic losses in the strips, and structures supporting current in the vertical direction [3], [9]. There is no limit on the number of ports extending from

Manuscript received February 18, 1992, revised September 15, 1993.

The authors are with the Department of Electrical Engineering, FT-10, University of Washington, Seattle, WA 98195

IEEE Log Number 9207408.

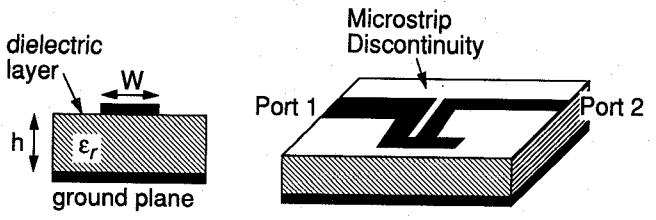

Fig. 1. Single layer microstrip geometry with a 2-port discontinuity.

the structure. The determination of current distribution as developed here does not require a lossless dielectric.

The arbitrary discontinuity or interconnect may be modeled through the method-of-moments (MOM) [6] applied to a relevant integral equation. We employ a mixed potential integral equation (MPIE) [3], which relates the current and charge densities on the upper conductor to the electric field incident upon that conductor. An alternative formulation is the dyadic electric-field integral equation (EFIE). In microstrip problems, however, this suffers from strong singularities in its Green's function. The MPIE also encounters singularities, but they are weak, rendering more stable and quickly convergent algorithms [9].

Solving the MPIE yields the surface currents from which S-parameters may be obtained. The MPIE for this problem may be written as two scalar equations,

$$-E_x^{inc} = -\jmath\omega \int_S dS' J_x(\bar{r}') G_a^{xx}(|\bar{r}' - \bar{r}|) - \frac{\partial}{\partial x} \int_S dS' q_s(\bar{r}') G_q(|\bar{r}' - \bar{r}|) \quad (1)$$

$$-E_y^{inc} = -\jmath\omega \int_S dS' J_y(\bar{r}') G_a^{yy}(|\bar{r}' - \bar{r}|) - \frac{\partial}{\partial y} \int_S dS' q_s(\bar{r}') G_q(|\bar{r}' - \bar{r}|), \quad (2)$$

where J_x and J_y are the transverse surface current densities on the upper conductor and q_s is the surface charge density. Green's functions G_a^{xx} and G_a^{yy} are, respectively, the x- and y-directed magnetic vector potentials for infinitesimal dipoles at the substrate/air interface. q_s is the surface charge density and Green's function G_q the scalar potential for a pulsating point-charge. While such isolated charges are non-physical, G_q is a useful mathematical device [9] for generating the scalar potential from a physical charge density q_s. E_x^{inc} and E_y^{inc} are the incident electric-fields and are zero except where the ports are driven.

In applying MOM to solve (1) and (2) and determine the surface currents, the interconnect and suitably long sections of its ports are subdivided into a rectangular grid whose subsections serve as domains for x- and y-directed current basis functions. The surface current densities on the upper conductor are expressed as

$$J_x(\bar{r}) = \sum_{j=1}^{N_x} c_{xj} b_{xj}(\bar{r}) \quad (3)$$

$$J_y(\bar{r}) = \sum_{j=1}^{N_y} c_{yj} b_{yj}(\bar{r}), \quad (4)$$

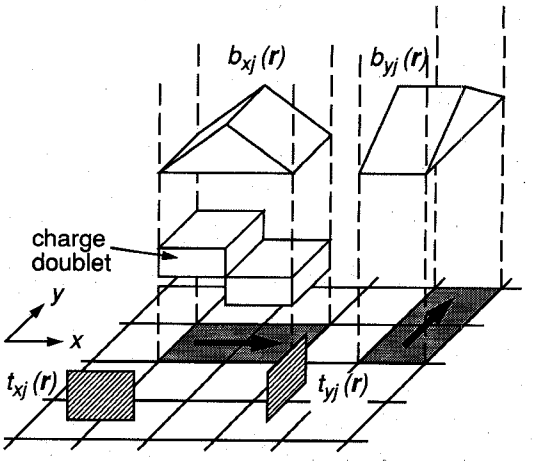

Fig. 2. Placement of roof-top basis functions and razor-blade testing functions in a rectangular grid.

where b_{xj} and b_{yj} are individual basis functions weighted by unknown coefficients c_{xj} and c_{yj}. N_x and N_y are the total number of current basis functions in each direction needed to fill out the geometry of the interconnect. We follow [10] in implementing this procedure, and the reader is referred to that paper for a full development and justifications. Briefly, we choose roof-top functions, shown in Fig. 2, for bases b_{xj} and b_{yj}. For $b_{xj}(\bar{r})$, each roof-top occupies two subcells in the x-direction and one subcell in the y-direction; the resulting distribution is piece-wise linear in the x-direction and stepped in the y-direction. A complementary arrangement exists for $b_{yj}(\bar{r})$.

By virtue of the continuity equation,

$$-\jmath\omega q_s = \frac{\partial J_x}{\partial x} + \frac{\partial J_y}{\partial y}, \quad (5)$$

the charge distribution is determined directly from these currents, giving a two-dimensional step distribution. With the charge now fixed in this manner, the triangular variation of each current basis is approximated by a pulse of equal height and half the length in the direction of current flow.

Basis function weights are found by using the MPIEs to construct a system of N linear equations where $N = N_x + N_y$. The fields are tested over each current segment by integrating both sides of (1) and (2) in conjunction with a set of N testing functions:

$$\langle -E_x^{inc}, t_{xj} \rangle = -\jmath\omega \langle A_x, t_{xj} \rangle - \langle \frac{\partial \Phi}{\partial x}, t_{xj} \rangle \quad (6)$$

$$\langle -E_y^{inc}, t_{yj} \rangle = -\jmath\omega \langle A_y, t_{yj} \rangle - \langle \frac{\partial \Phi}{\partial y}, t_{yj} \rangle, \quad (7)$$

where

$$\langle a, b \rangle = \int dx\, dy\, a(x,y)\, b(x,y). \quad (8)$$

A_x, A_y and Φ are the vector and scalar potentials represented as integrals in (1) and (2). As in [10], we employ razor-blade functions t_{xj} and t_{yj}, shown in Fig. 2. In the

x-direction, $t_{xj}(\bar{r})$ is a pulse running from the center of one subcell to the center of the next subcell; its y-dependence is an impulse function. A similar description holds for t_{yj}. The unknown coefficients c_{xj} and c_{yj} of (3) and (4) are transferred outside of the integration. Equations (6) and (7) are expressed in matrix form as

$$\begin{bmatrix} V_x \\ V_y \end{bmatrix} = \begin{bmatrix} Z_{xx} & Z_{xy} \\ Z_{yx} & Z_{yy} \end{bmatrix} \begin{bmatrix} C_x \\ C_y \end{bmatrix} \tag{9}$$

where V_x and V_y are vectors whose elements v_{xj} and v_{yj} are the left-hand side of (6) and (7). These are set to zero except where testing functions coincide with locations of port excitation; here they are set to a constant, corresponding to a horizontal voltage source. The impedance matrix Z roughly corresponds to the mutual impedances between the current elements. It is divided into co-polarized and cross-polarized contributions, the latter being generated only through the contribution of scalar potential, Φ. C_x and C_y are vectors containing the coefficients c_{xj} and c_{yj}.

The scalar potential contribution in (6) and (7) involves a partial derivative of the scalar Green's function G_q. This potential is computed numerically, so we employ the usual procedure of transferring the derivative to the testing function through integration by parts. The derivative of the razor blade function is a pair of oppositely signed impulse functions; thus, the contribution of the scalar potential becomes the difference in scalar potentials sampled in the center of adjacent subcells.

B. Efficient Evaluation of Green's Function

With microstrip geometries, the most difficult aspect of generating the elements for impedance matrix Z in (9) is the evaluation of the Green's functions G_a and G_q. They are commonly expressed as Sommerfeld-type integrals [11], inverse Hankel transforms of the spectral-domain Green's function. Closed-form spectral Green's functions can be generated for multiple layer dielectrics over a ground plane through equivalent transmission line analysis [12], [13]. For the single layer geometry of Fig. 1, the spectral Green's functions with the source and observation point at the free-space/dielectric interface are given by [8]

$$\tilde{G}_a^{xx} = \frac{\mu_o}{4\pi} \frac{1}{j2k_{zo}} e^{-jk_{zo}} [1 + R_{TE}(k_\rho)] \tag{10}$$

$$\tilde{G}_q = \frac{1}{4\pi\epsilon_o} \frac{1}{j2k_{zo}} e^{-jk_{zo}} [1 + R_{TE}(k_\rho) + R_q(k_\rho)], \tag{11}$$

where ϵ_o and μ_o are the free-space permittivity and permeability. Wavenumbers k_{zo} and k_ρ are the z- and ρ-components of free-space propagation constant k_o. Reflection coefficients R_{TE} and Rq account for the effect of the substrate over the ground plane. The reader is referred to [8] for a full exposition of these equations.

The spatial Green's functions can now be written as

$$G_{a,q}(\rho) = \int_{-\infty}^{+\infty} \tilde{G}_{a,q} H_0^2(k_\rho \rho) k_\rho \, dk_\rho \tag{12}$$

where ρ is the displacement between the source and the observation point. While these Sommerfeld integrals for G_a^{xx} and G_q may be evaluated efficiently through analytic approximations in the near- and far-field [11], intermediate regions require quadrature with slowly convergent, oscillatory integrands. However, a technique developed in [7] and improved in [8] allows highly efficient evaluation in all regions. Briefly, the Sommerfeld integral can be separated into three contributions: 1) quasi-dynamic images, 2) surface waves and 3) complex images. The first two contributions, which dominate respectively in the near- and far-fields, are extracted from R_{TE} and R_q and handled analytically. What remains in R_{TE} and R_q is sufficiently well-behaved to be approximated by a short series of exponentials whose exponents and weights are computed using Prony's method [14]. Our experience shows that two to four terms, depending on the frequency, are appropriate for this expansion. The inverse Hankel transforms involving these exponentials are then handled analytically. Particular care should be given in the selection of the number of expansion terms for Gq since its contribution in (6) and (7) is a second-order difference, one from the pulse doublet and one from the testing procedure.

Our experience shows that this process yields about a 100 fold reduction in computation time for the multiple evaluations of potentials in computing the inner products of (6) and (7) and was instrumental in reducing the time spent filling the impedance matrix to the point where it no longer dominated the computation time in the MOM procedure.

III. Extraction of Scattering Parameters

The scattering parameters of an interconnect are extracted by introducing a combination of excitations at the port ends and examining the current distribution on the ports. Excitation is provided by horizontal voltage sources spanning the width of the port end and directed along its length [1], [15]. In this scheme, the port ends are terminated in "open-circuits", which can be represented by an equivalent impedance. The reader may observe that this is not the approach normally used in practice of a wave induced from a matched source. Further, the definition of the individual S-parameters assumes no reflections at the port end. Still, this method is viable because the relationships among the current waves entering and leaving the interconnect ports are governed exclusively by the interconnect S-parameters. In other words, having open-circuited port ends instead of matched termination will change the current distribution but not these relationships. By applying a sufficient number of unique excitations, the S-parameters can be determined without direct knowledge of the effects of the open-circuit port terminations.

For an arbitrary N-port discontinuity, N linearly-independent excitation combinations are required. The computed current distributions for each excitation and on each port are fit to a unimodal transmission line form [16]:

$$I(x) = ae^{-\gamma x} - be^{\gamma x}, \tag{13}$$

where x is the position along the line. $I(x)$ is the current distribution on the port, obtained by integrating J_x across its

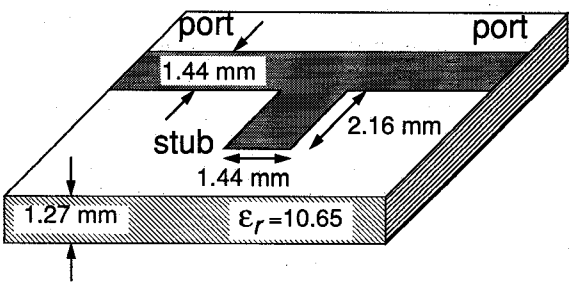

Fig. 3. Dimension and substrate parameters of microstrip stub and attached uniform line.

width. a and b are the complex amplitudes wave amplitudes. Complex propagation constant γ is prior obtained by MOM analysis of the uniform line(s).

In fitting the current distribution to the unimodal-propagation model, samples near the port ends and the discontinuity should be left out owing to the presence of higher-order modes. The S-parameters are then obtained from the computed wave amplitudes by relating them through a system of N equations.

If the S-parameters are to be employed in a circuit analysis, it will also be necessary to know the characteristic impedances of the ports. The uniform line has been extensively studied, and impedances can be most easily obtained from established closed-form formulas [17].

A. Validation

We demonstrate the validity of this procedure by modeling a microstrip stub whose S-parameters have been measured [1]. The substrate and stub dimensions are given in Fig. 3. In the MOM procedure, a uniform discretization with a 0.24 × 0.24 mm subcell is selected and the length of the transmission line set to 102 subcells or 24.48 mm. For the transmission line alone, there are 101 × 6 x-directed and 102 × 5 y-directed current basis functions. The entire structure requires a total of 1215 basis functions. Taking advantage of the redundancy in a uniform discretization and the efficient algorithms for computing Green's functions described above, the evaluation of the elements for the 1215 × 1215 matrix requires 2.5 CPU minutes on on a VAX-6000-530 computer, much shorter than the 30 CPU minutes required to reduce the matrix using LINPACK.

The structure is analyzed from 7.5 to 12 GHz. The transmission S_{12} computed by MOM and Libra ver. 3.000 is compared with measurement in Fig. 4. Measurement and MOM show the stub resonance near 10.15 GHz while Libra predicts a resonance at 9 GHz. The stub is modeled in Libra with a microstrip TEE element attached to a section of open-circuited line with capacitive edge-effect. These elements are operated within specified regions of validity [18].

IV. Circuit Simulation

To demonstrate the importance of accurate characterization of interconnects, we analyze the single-stage amplifier in Fig. 5. The active device is a GaAs MESFET connected to the microstrip meander on the same substrate. Both AC small-signal and large-signal, harmonic balance analyses are

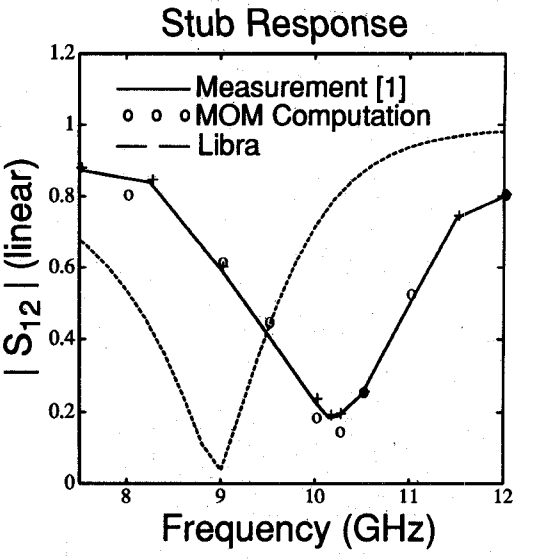

Fig. 4. Computed (Method-of-Moments, Libra v 3.000) and measured transmission responses of stub.

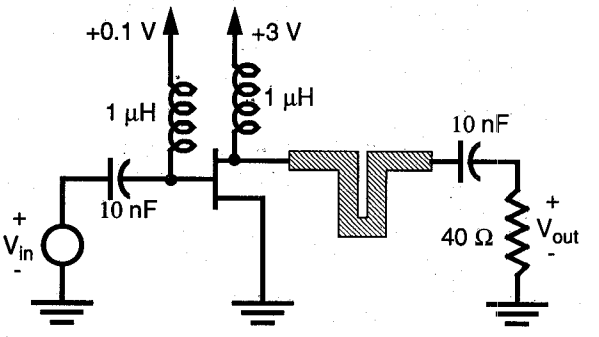

Fig. 5. Single-stage microwave amplifier.

performed using MISIM (Model-Independent Simulator) [19]. Harmonic balance [20] is a frequency-domain technique for steady-state simulation of systems containing nonlinear devices. Typical passive element properties such as frequency dependent behavior are directly processed, while nonlinearities of the active devices are handled through the FFT conversion of the time-domain device equations. The computed response is interpreted as harmonic distortion. In these frequency-domain analyses, the meander is treated as a two-port network characterized by its S-parameters, which are converted into Y-parameters for circuit simulation.

The dimensions of the meander and gallium-arsenide substrate are given in Fig. 6. The meander is initially discretized into 0.333 × 0.333 mm subcells. The ports extend 80 subcells in the model in order to collect current samples over a sufficient portion of a wavelength at lower frequencies. This level of discretization is adequate for analysis from 1 GHz to 4 GHz. Beyond 4 GHz, a 0.1665 × 0.333 mm subcell is used in order to generate an adequate number of current samples per wavelength on the ports.

Results for full-wave analysis of the meander are given in Fig. 7. The meander is also modeled on Libra ver. 3.000 using a combination of corner bends and coupled lines. It should be noted that the corner bend elements are being

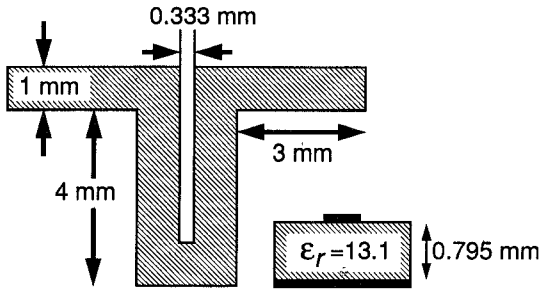

Fig. 6. Dimensions and substrate parameters of microstrip meander.

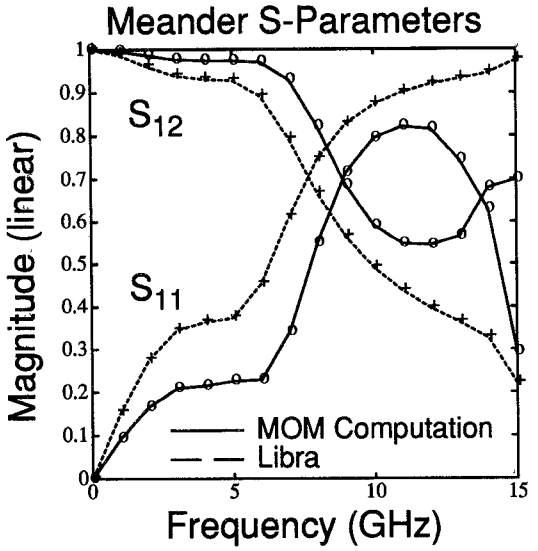

Fig. 7. 2-port parameters of symmetric meander computed by MOM and Librav 3.000.

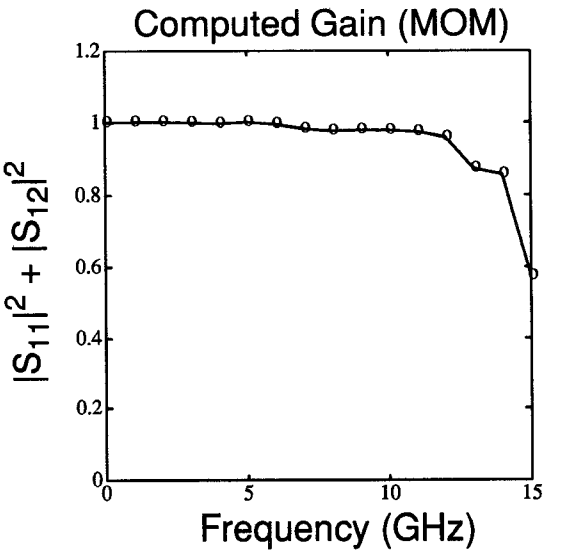

Fig. 8. MOM computed gain of microstrip meander, showing significant radiation loss at higher frequencies.

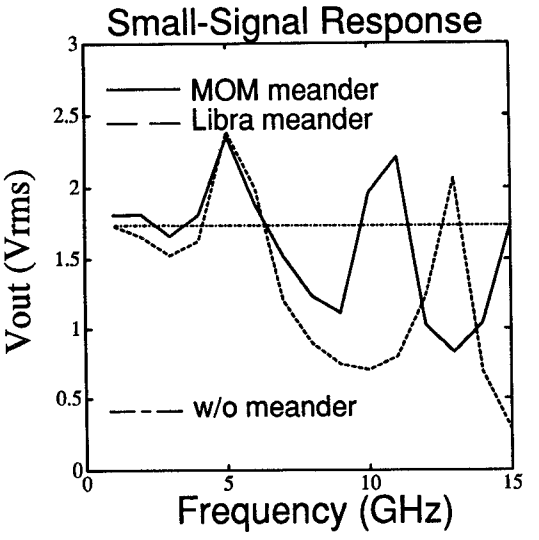

Fig. 9. Amplifier small-signal gain with MOM and Libra characterizations of the meander and with microstrip meander absent.

applied beyond the stipulated range of validity as specified in the *EEsof Element Catalog* [18]: $\varepsilon_r < 10.4$; no applicable substitute could be found. A reference impedance of 38.5 ohms is specified to generate S-parameters, a value determined as representative at lower frequencies using LINECALC. The response predicted by MOM and Libra diverge with increasing frequency. With Libra, the gain $|S_{11}|^2 + |S_{12}|^2$ is always unity, suggesting a model which does not account for radiation. The full-wave model, however, shows gain in Fig. 8 trailing off, an effect which can be attributed to radiation both in the space above the dielectric and trapped along the dielectric as a surface wave [21].

The MISIM computed small-signal response of the amplifier is given in Fig. 9. The source V_{in} is stepped in frequency from 1 to 15 GHz. The difference in predicted meander performance by MOM and Libra is manifest at higher frequencies in the resulting amplifier gain responses $|\frac{V_{out}}{V_{in}}|$. For reference, the small-signal response with the meander removed is also shown.

Large-signal simulations for 1, 3, and 5 GHz driving frequencies are shown in Fig. 10(a). For each frequency, the source has an amplitude of 0.4 volts peak-to-peak. The harmonic spectra computed from harmonic-balance are Fourier transformed to render steady-state time responses. Signals V_{out} are traced over one cycle at each frequency for the amplifier with the meander characterized both by MOM and Libra. The large-signal responses with the meander removed are given in Fig. 10(b). In this case, the signals are nearly identical. The MESFET is overdriven, producing clipping distortion at the output. At 1 GHz, the full-wave and Libra based amplifier simulations are in good agreement. As the frequency is increased to 5 GHz, however, pronounced differences appear in the predicted distortion. While meander characterizations by Libra and MOM are comparable at 5 GHz, clipping produces significant energy in the harmonics at 10 and 15 GHz, where MOM and Libra diverge.

V. Conclusion

In this paper, we have demonstrated a technique for full-wave analysis of microstrip interconnects and its integration with microwave circuit simulation.

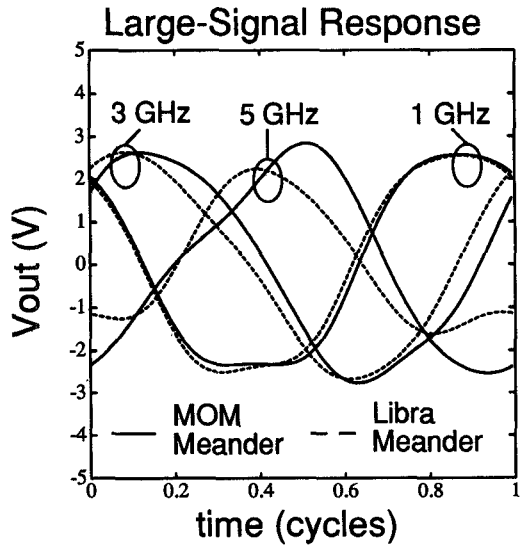

(a)

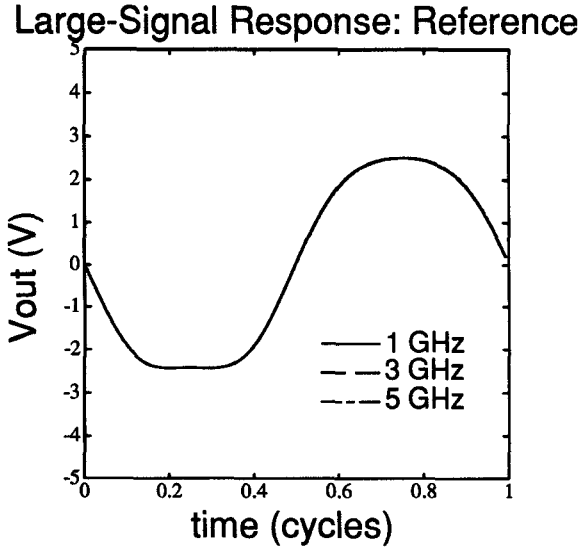

(b)

Fig. 10. Time-domain amplifier output computed using harmonic-balance analysis with 0.4 volt p-p (large-signal) input at 1, 3 and 5 GHz: (a) responses with MOM and Libra characterization of the meander, and (b) responses with microstrip meander absent.

A description was given of interconnect modeling through application of the method-of-moments to a mixed-potential integral equation. We employed a recently published algorithm for efficient and accurate evaluation of microstrip Green's functions, demonstrating that for uniform discretization in the MOM procedure, impedance matrix fill-time can be reduced to the point where matrix solve-time is dominant.

The importance of full-wave analysis was demonstrated in the case of a microstrip stub, where our overall procedure compared favorably with experimental data available in the literature. Results from a modern commercial microwave CAD package compared less favorably.

Small- and large- signal analyses were applied in simulating a single-stage amplifier circuit. The circuit incorporated a meander microstrip section whose characteristics were predicted by both full-wave analysis and a microwave CAD package. With small-signal analysis, differences in characterizing the meander were manifest in the amplifier response at higher frequencies. When driven at lower frequencies with a large signal, harmonics generated by the amplifier at higher frequencies resulted in different distortion phenomena amongst the two meander representations.

ACKNOWLEDGMENT

This work was partially supported by the NSF (ECS-9158040) and NSF Center for the Design of Analog/Digital Integrated Circuits (CDADIC).

REFERENCES

[1] W. P. Harokopus and Jr., L. P. B. Katehi. Characterization of microstrip discontinuities on multilayer dielectric substrates including radiation losses. *IEEE Trans. Microwave Theory Tech* , MTT-37(12):2058–2066, Dec. 1989.

[2] R. W. Jackson. Full-wave, finite-element analysis of irregular microstrip discontinuities. *IEEE Trans. Microwave Theory Tech.*, MTT-37(1):81–89, Jan. 1989,

[3] J. R. Mosig. Arbitrarily shaped structures and their analysis with a mixed potential integral equation. *IEEE Trans. Microwave Theory Tech.*, MTT-36(2):314–323, Feb. 1988

[4] D. M. Sheen, S. M. Ali, M. D. Abouzahra and J. A. Kong. Application of the three-dimensional finite-difference time-domain method to the analysis of planar microstrip circuits. *IEEE Microwave Theory Tech.*, MTT-38(7):849–857, July 1990.

[5] J. R. Mosig and F. E. Gardiol. General integral equation formulation for microstrip antennas and scatters. *IEE Proc.*, vol. 132-H(7):424–432, Dec. 1985.

[6] R. F. Harrington. *Field Computation by Moments Methods.* Macmillan, New York, 1968.

[7] D. G. Fang, J. J. Yang, and G. Y. Delisle. Discrete image theory for horizontal electric dipoles in a multilayered medium above a conducting ground plane. *Proc. IEE*, vol. 135-H:297–303, 1988.

[8] Y. L. Chow, J. J. Yang, D. G. Fang and G. E. Howard. A closed-form spatial Green's function for the thick microstrip substrate. *IEEE Trans. Microwave Theory Tech.*, MTT-39(3):588–592, March 1991

[9] J. R. Mosig. Integral equation techniques for the dynamic analysis of microstrip discontinuities. *Alta Frequenza*, vol. 57(5):171–181, June 1988.

[10] A. W. Glisson and D. R. Wilton. Simple and efficient numerical methods for problems of electromagnetic radiation and scattering from surfaces. *IEEE Trans. Antennas Propagat.*, AP-28(5):593–603, Sep. 1980.

[11] J. R. Mosig and F. E. Gardiol. Analytical and numerical techniques in the Green's function treatment of microstrip antennas and scatterers. *IEE Proc.*, vol. 130-H(2):175–182, March 1983

[12] T. Itoh. Spectral-domain immittance approach for dispersion characteristics of generalized printed transmission lines. *IEEE Trans. Microwave Theory Tech.*, MTT-28(7):733–737, July 1980

[13] A. Sommerfeld. *Partial Differential Equations in Physics.* Academic Press, New York, 1949.

[14] F. B. Hildebrand. *Introduction to Numerical Analysis.* McGraw-Hill, New York, 1974, pp. 457–465.

[15] L. P. B. Katehi and N. G. Alexopoulos. Frequency-dependent characteristics of microstrip discontinuities in millimeter-wave integrated circuits. *IEEE Microwave Theory Tech.*, MTT-33(10):1029–1035, Oct. 1985

[16] T. G. Livernois and P. B. Katehi. A simple method for characterizing planar transmission line discontinuities on dissipative substrates. *IEEE Microwave Theory Tech.* , MTT-39(2):368–370, Feb. 1991

[17] I. Bahl and P. Bhartia. *Microwave Solid State Circuit Design.* John Wiley & Sons, New York, 1988, pp. 16–19.

[18] EEsof Inc. *EEsof element catalog.* EEsof Inc., California, 1989.

[19] A. T. Yang, C. H. Chan, J. T. Yao, R. R. Daniels and J. P. Harrang. Modeling and simulation of high-frequency integrated circuits based on scattering parameters. *Proc. 28th ACM/IEEE Design Automation Conference*, pp. 727–757, 1991.

[20] K. S. Kundert and A. Sangiovanni-vincentelli. Simulation of nonlinear circuits in the frequency domain. *IEEE Trans. Computer Aided Design*, CAD-5:521-555, 1986.

[21] W. P. Harokopus, Jr., L. P. B. Katehi, W. Ali-Ahmad, and G. M. Rebeiz. Surface-wave excitation from open microstrip discontinuities. *IEEE Trans. Microwave Theory Tech.*, MTT-39(7):1098–1107, July 1991.

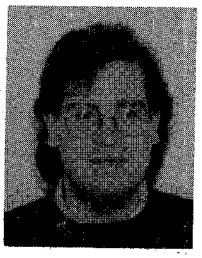

Robert Kipp was born in Berwyn, Illinois in 1965. He received the B.S.S.E.E. and B.S. Mathematics from Rose-Hulman Institute of Technology in 1987 and the M.S.E.E. from the University of Washington in 1990. From July 1988 to December 1989, he was employed by the Boeing Co. as an electromagnetics engineer.

He is presently pursuing a Ph.D. degree at the University of Washington, where he works in the Electromagnetics and Remote Sensing Laboratory as a research assistant. His research involves modeling of microstrip discontinuities and frequency selective surfaces.

Chi H. Chan attended Hong Kong Polytechnic and the City College of New York. He received the B.S. and M.S. degree in electrical engineering from Ohio State University, Columbus, Ohio, in 1981 and 1982, respectively, and the Ph.D. degree in electrical engineering from the University of Illinois, Urbana, Illinois, in 1987.

From 1981 to 1982, he was a Graduate Research Associate at the ElectroScience Laboratory, Ohio State University. From 1987 to 1989, he was a Visiting Assistant Professor at the University of Illinois. In September 1989, he joined the University of Washington, Seattle, Washington as an Assistant Professor. His research interests include numerical techniques in electromagnetics, frequency-selective surfaces, microwave integrated ciccuits, high-speed digital circuits, wave propagation in anisotropic media for integrated optics applications, finite-element and finite-difference methods for remote sensing and biomedical applications, and neural-networks techniques for inverse scattering and antenna designs.

Chi Chan is a member of URSI Commission B and a recipient of the 1991 NSF Presidential Young Investigator award.

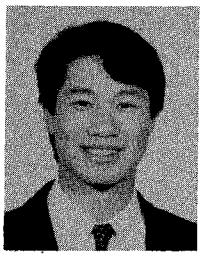

Andrew T. Yang received the B.S. degree in electrical engineering and computer science from the University of California at Berkeley in 1983, and the M.S. and Ph.D. from the University of Illinois at Urbana-Champaign in 1986 and 1989, respectively. He is currently an Assistant Professor of Electrical Engineering at the University of Washington.

Dr. Yang's research interests have been in the areas of modeling and simulation of analog/digital circuits, high-performance circuits with complex nonlinear effects, and optoelectronic integrated circuits. Dr. Yang is currently serving as the co-editor of Modeling and Simulation for *IEEE Design and Test Magazine*. He has been a member of the technical program committee for the *IEEE International Conference on Computer-Aided Design*.

Dr. Yang received the NSF National Young Investigator Award in 1992.

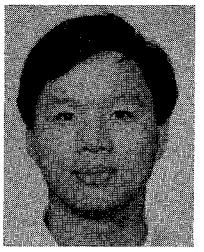

Jack Tzu-Wen Yao was born in Taipei, Taiwan, on July 14, 1962. He received the B.S. degree in physics from National Taiwan University in 1984 and the M.S. degree in electrical engineering from the University of Massachusetts at Lowell in 1987.

From 1984 to 1987, he was with the semiconductor group of Texas Instruments Inc. in Taipei, Taiwan. Since 1989 he has been a research assistant in the Design-Test-Reliability Laboratory at the University of Washington, Seattle, WA, where he is pursuing his Ph.D degree. His research interests are in the area of non-linear high-frequency CAD. He currently has a Tektronix Student Research Fellowship.